

RESEARCH

Open Access



The anterior gradient homologue 2 (AGR2) co-localises with the glucose-regulated protein 78 (GRP78) in cancer stem cells, and is critical for the survival and drug resistance of recurrent glioblastoma: in situ and in vitro analyses

Deema Hussein^{1,2*†}, Reem Alsereihy^{1,3,4†}, Abdulla Ahmed A. Salwati¹, Rinad Algehani¹, Alazouf Alhowity¹, Ahmed M. Al-Hejin³, Hans-Juergen Schulten⁵, Saleh Baeesa⁶, Mohammed Bangash⁶, Fahad Alghamdi⁷, Richard Cross⁸, Torki Al Zughaihi^{1,2}, Mohamad Saka^{1,2}, Adeel Chaudhary^{2,9} and Adel Abuzenadah^{1,2,5,9}

Abstract

Background: Glioblastomas (GBs) are characterised as one of the most aggressive primary central nervous system tumours (CNSTs). Single-cell sequencing analysis identified the presence of a highly heterogeneous population of cancer stem cells (CSCs). The proteins anterior gradient homologue 2 (AGR2) and glucose-regulated protein 78 (GRP78) are known to play critical roles in regulating unfolded protein response (UPR) machinery. The UPR machinery influences cell survival, migration, invasion and drug resistance. Hence, we investigated the role of AGR2 in drug-resistant recurrent glioblastoma cells.

Methods: Immunofluorescence, biological assessments and whole exome sequencing analyses were completed under in situ and in vitro conditions. Cells were treated with CNSTs clinical/preclinical drugs taxol, cisplatin, irinotecan, MCK8866, etoposide, and temozolomide, then resistant cells were analysed for the expression of AGR2. AGR2 was repressed using single and double siRNA transfections and combined with either temozolomide or irinotecan.

Results: Genomic and biological characterisations of the AGR2-expressed Jed66_GB and Jed41_GB recurrent glioblastoma tissues and cell lines showed features consistent with glioblastoma. Immunofluorescence data indicated that AGR2 co-localised with the UPR marker GRP78 in both the tissue and their corresponding primary cell lines. AGR2 and GRP78 were highly expressed in glioblastoma CSCs. Following treatment with the aforementioned drugs, all drug-surviving cells showed high expression of AGR2. Prolonged siRNA repression of a particular region in AGR2 exon 2 reduced AGR2 protein expression and led to lower cell densities in both cell lines. Co-treatments using AGR2 exon 2B siRNA in conjunction with temozolomide or irinotecan had partially synergistic effects. The slight reduction of

[†]Deema Hussein and Reem Alsereihy are Co-first authors

*Correspondence: dmhussein@kau.edu.sa; deemah@hotmail.com

¹ King Fahd Medical Research Center, King Abdulaziz University, 80216, Jeddah 21589, Saudi Arabia

Full list of author information is available at the end of the article



AGR2 expression increased nuclear Caspase-3 activation in both cell lines and caused multinucleation in the Jed66_GB cell line.

Conclusions: AGR2 is highly expressed in UPR-active CSCs and drug-resistant GB cells, and its repression leads to apoptosis, via multiple pathways.

Keywords: Glioblastoma, Cancer stem cells (CSCs), Anterior gradient homologue 2 (AGR2), Glucose-regulated protein 78 (GRP78), Drug resistance

Introduction

Glioblastomas are characterised as grade 4, and are highly aggressive primary central nervous system tumours (CNSTs) [1]. Tumours are often devastating, and they have a poor prognosis and a limited survival time of approximately 2.4 years [2, 3]. The optimal treatment for glioblastomas is complete resection through surgery. However, for inoperable tumours, other treatments are used, including radiation and cytotoxic chemotherapy. For incomplete surgical resection, a median survival of 12–15 months after diagnosis, and a less than 5% of patients surviving more than 5 years have been reported [4].

A whole bulk DNA analysis of glioblastoma tissues led to the identification of mutations in isocitrate dehydrogenase 1/2 (*IDH1/2*), phosphatase and tensin homolog (*PTEN*), cyclin dependent kinase inhibitor 2A (*CDKN2A*), tumour protein p53 (*TP53*), parkin RBR E3 ubiquitin protein ligase (*Park2*), protein tyrosine phosphatase receptor type D (*PTPRed*) and neurofibromin 1 (*NF1*) genes. Several amplifications of genes have also been identified including the amplifications of the epidermal growth factor receptor (*EGFR*), fibroblast growth factor receptor 2 (*FGFR2*), insulin receptor substrate 2 (*IRS2*), and AKT serine/threonine kinase 3 (*AKT3*) [5]. In contrast, single-cell sequencing experiments highlighted a high level of inter- and intra-patient heterogeneity [6, 7]. Further work supported vast differences in the genetic profiles of different glioblastoma patients and showed a remarkably high plasticity between different cell types within a tumour [8, 9].

Single cell sequencing analysis also identified a high heterogeneity of cancer stem cells (CSCs) within glioblastomas [7, 9]. CSCs are cancer cells that utilise stem cell pathways to promote tumour growth and are linked with aggressiveness and treatment resistance [10, 11]. Stem cell associated pathways have recently been classified as a new hallmark of cancer referred to as “Unlocking Phenotypic Plasticity” [12]. Glioblastoma CSCs express numerous markers [13, 14]. However, a single marker is insufficient to indicate the presence of CSCs, rather it is the expression of multiple CSC markers that is indicative of the presence of these cells [14, 15].

The unfolded protein response (UPR) machinery resides in the endoplasmic reticulum (ER) and is responsible for the degradation of misfolded proteins. UPR is triggered in normal cells via the increased expression of ER proteins and their localisation to the ER [16]. In cancer cells, this machinery is deregulated as the accumulation of misfolded/unfolded proteins increases greatly [17]. Glucose-regulated protein 78 (GRP78), also known as heat shock protein A5 (HSPA5) or binding immunoglobulin protein (BIP), is a critical UPR marker that acts as an ER molecular chaperone and modulates the UPR machinery [18]. GRP78 was found to be highly expressed in glioblastomas [19, 20], and several studies have demonstrated that its increased expression enhances cell survival, migration, invasion, and drug resistance [21–23].

A partner of the GRP78 protein is the anterior gradient homologue 2 (AGR2), which was shown to inhibit the UPR-endoplasmic reticulum associated protein degradation (ERAD) process [24]. The *AGR2* gene is located in chromosome7p21.3; it has 8 exons, and transcribes six splice variants: *AGR2vC*, *AGR2vD*, *AGR2vE*, *AGR2vF*, *AGR2vG*, and *AGR2vH* [25]. *AGR2* is highly expressed in the stomach, colon and duodenum; however, it is not expressed in normal brain tissues [26, 27]. Knockout experiments in mice showed that *AGR2*^{-/-} mice poorly develop inner colon mucus layers [28], have deformed tissue regeneration [29], and develop severe acute terminal ileitis with multinucleated giant cells reminiscent of granulomatous inflammation [30]. In cancer cells, the protein was shown to be upregulated in several aggressive types including glioblastoma [31, 32], and it was found to colocalise with CSC markers in high-grade tumours [31, 33–35]. Secreted *AGR2vH*, which can be detected in the blood and urine of cancer patients, was shown to contribute to metastasis [15, 36–38].

To date, the contribution of GRP78 and *AGR2* to drug resistance in CSCs of glioblastoma tissues and primary cell lines has not been clarified. In the present study, we determined the levels of the *AGR2* protein expression in recurrent glioblastoma tissues and primary cell lines, and explored its co-expression with GRP78 and several CSC markers. We further investigated the relationship between *AGR2* expression and drug resistance for clinically/preclinically known chemotherapeutics, and

assessed the effects on cell survival upon repression of AGR2 using small interfering RNA (siRNA) sequences in combination with chemotherapeutic drugs.

Methods

Tissue and cell line retrieval

The examined tissues and cell lines were recurrent primary glioblastoma tumours obtained from the Neurooncology Translational Group at King Fahad Medical Research Center for patients who were treated at King Abdulaziz University Hospital. The Jed66_GB cell line was retrieved from a recurrent adult-type glioblastoma, IDH1/2-wild type, World Health Organisation (WHO) grade 4, from a 32-year-old male. The Jed41_GB cell line was retrieved from a recurrent tumour of a 5-year-old boy diagnosed with glioblastoma, giant cell variant, IDH1/2-wild type, WHO grade 4, Additional file 1: Figure S1 (Data retrieved from whole exome sequencing showed no damaging variants for IDH1/2). The samples were recovered and cultured as previously described [39]. For all experiments, early passages up to passage 35 were used to ensure that both cell line models remained genomically similar to the original tumours.

Biological assessments

To assess the clonogenic capacity, cells were plated in 6-well plates at different cell numbers and were cultured to form clones. 14 to 21 days following seeding, clones were fixed with 4% paraformaldehyde (PFA), then stained with crystal violet, and counted. All experiments were carried out in biological triplicate. To track migratory progression, scratch assay experiments were performed as previously described [39]. Briefly, cells were plated in 6-well plates, left to adhere overnight and a scratch 'wound' was made using a 10 µl pipette tip when the cells reached 80% confluency, and cells' movements were followed up for 3–4 days. Cell monitored at 5 × magnification using a digital microscope camera (Leica DFC425).

DNA whole exome and conventional sequencing of tissue and cell lines

DNA was extracted from the tissues and corresponding cell lines (Jed66_GB cell line passage 22 and Jed41_GB cell line passage 25) (DNeasy Blood & Tissue Kit, 69504, Qiagen), and whole exomes were sequenced using Agilent, UAE services. VCF files were annotated using the BaseSpace Variant Interpreter (Illumina, San Diego, CA) (accessed on the 05/12/2021). Only those COSMIC variants that had damaging coding consequences were further assessed, as called by BaseSpace Variant Interpreter, or checked manually using PolyPhen-2 Wiki. They had a population frequency of less than 0.01 for all population sources. COSMIC variants detected in the tissues and

corresponding cell lines were selected to enrich the tumorigenic and progressive genes. One critical exon variant in *STC2* in Jed66_GB and one in *TP53* in Jed41_GB were assessed by conventional sequencing that was performed on tissue and corresponding cell lines as described in our standard protocol [40]. The primers used for PCR amplification and sequencing were for *STC2*-exon 4 [forward and reverse primer sequences (3'-5'): TGA GCGAGGTAGCAAGAG and CGATGAAGTCCACAG TCC]; and *TP53* in intron 8-exon9 [forward and reverse primer sequences (3'-5'): TTCCTTACTGCCTCTTGC, and GCTTCTTGTCCTGCTTGC]. The specificity of the PCR products was ascertained by gel electrophoresis. Subsequently, the PCR products were purified and underwent cycle sequence reactions using a BigDye Terminator V3.1 Cycle Sequencing Kit (Thermo Fisher Scientific Inc., Waltham, MA). The purified sequencing products were finally resolved with capillary electrophoresis (3130 Genetic Analyzer, Thermo Fisher Scientific Inc., Massachusetts, USA).

Immunofluorescence staining

To process in situ immunofluorescence, tissue sections were fixed and stained as previously described [15]. For the cell line immunofluorescence staining, the cells were seeded on chamber slides, fixed and stained as previously described [39]. The rabbit primary antibodies used in this study were anti-AGR2 (1:100, ab76473, raised against AGR2 exon 2, abcam), anti-Ki67 (1:200, ab16667, abcam), anti-SRY-box transcription factor 2 (SOX2) (1:200, 09-0024, Miltenyi), anti-Frizzled 9 (FZD9) (1:100, ab150515, abcam), anti-gliial fibrillary acidic protein (GFAP) (1:500, ab7260, abcam), anti-oligodendrocyte transcription factor 2 (OLIG2) (1:500, ab42453, abcam), anti-tubulin beta 3 class III (TUBB3) (1:100, ab18207, abcam), and anti-Caspase-3 (1:100, ab40a51, abcam). The mouse primary antibodies used in this study were anti-GRP78 (1:50, ab181499, abcam), anti-BMI1 proto-oncogene, polycomb ring finger (BMI1) (1:100, ab14389, abcam), anti-Nestin (1:50, ab6142, abcam), anti-Vimentin (VIM) (1:100, ab8978, abcam), anti-stage-specific embryonic antigen-4 (SSEA4) (1:100, ab16287, abcam), anti-prominin 1 (CD133) (1:100, W6B3C1, Miltenyi), and anti-tumour protein p53 (P53) (1:100, ab26, abcam). For secondary goat antibodies, 488 anti-mouse (1:300, ab150105, abcam) and 555 anti-Rabbit (1:700, ab150074, abcam) antibodies were used. Vectashield with DAPI was added to stain the nuclei. Pictures were taken at 20 × magnification using a Leica DMI6000 microscope and a Leica DFC425 camera and they were processed as previously described [15, 39].

Clonogenic cytotoxic assay and growth inhibition

Several drugs were used in this study. Taxol, a microtubule stabiliser (T7402, Sigma, dissolved in DMSO); cisplatin, a DNA cross-linker (P4394, Sigma, dissolved in saline); irinotecan, a DNA topoisomerase I inhibitor (I1406, Sigma, dissolved in DMSO); MCK8866, IRE1 α inhibitor (HY-104040, MCE, dissolved in water); etoposide, DNA topoisomerase II inhibitor (E1383, Sigma, dissolved in DMSO); and temozolomide, DNA guanine and adenine methylation agent (HY-17364, MCE, dissolved in DMSO).

For the clonogenic cytotoxic assay, cells were plated in 6-well plates at 1,000 and 2,000 cells per well for Jed66_GB and Jed41_GB, respectively. Cells were supplemented with DMEM-F12 and 10% FBS and left to adhere overnight at 37 °C with 5% CO₂. On the next day, cells were treated for two hours with either cisplatin or etoposide, or for three days with either taxol, or irinotecan or MCK8866. 14 to 21 days following seeding, the clones were fixed with 4% PFA, stained with crystal violet and counted.

To determine the IC₅₀ values for temozolomide and irinotecan in order to use for growth inhibition assays, cells were plated in 96-well plates at 5×10^3 or 1×10^4 cells/well for Jed66_GB and Jed41_GB, respectively. For temozolomide, the concentrations used were 50, 100, 200, 400, 800, 1600, and 3200 μ M for both cell lines. For irinotecan the concentrations 0.5, 1, 2, 4, 8, and 16 μ M were used to treat Jed66_GB, while for Jed41_GB higher concentrations were required (25, 50, 100, 200, 400, 800 μ M). After three days of drugs incubation, the cells were fixed with 4% PFA, stained with 1% crystal violet, and the absorbance was measured at 595 nm. All assays were performed in triplicate.

siRNA transfections

For basic transfection optimisation, cells were seeded in 8-well chamber slides at 2×10^4 cells/well and 4×10^4 cells/well for Jed66_GB, and Jed41_GB, respectively and were left overnight to attach in 400 μ L Transfection Media (TM) (DMEM-F12 media with 10% FBS and no antibiotics). The following day, cells were transfected with 0.6% or 1.0% of lipofectamine (Lipofectamine[®]RNAiMAX, 13778075, Integrated DNA Technology), or with 0.2% or 0.3% of Cy3-DsiRNA (CY3 DS Transfection Control, 77619141, Integrated DNA Technology), or with 0.2% or 0.3% of the negative control (DsiRNA-Negative Control, 77619142, Integrated DNA Technology). Cell death was at 80% using 1% lipofectamine concentration in initial experiments; therefore, the concentration of 0.6% lipofectamine was used for further AGR2 siRNA experiments.

To optimise AGR2 repression using a single transfection, three siRNAs targeting different exon sequences were tested at a final concentration of 0.2% (Integrated DNA Technologies, Coralville, IO). The siRNA sequences were as follows: AGR2 exon 2A siRNA (5'-AGAUACCACAGUCAAAACCUGGAGCCAAA-3') (hs.Ri.AGR2.13.5, Integrated DNA Technology), AGR2 exon 2B siRNA (5'-AAAGGACUCUCGACCCAAACUGCCCC-3') (Customised, Integrated DNA Technology) and AGR2 exon 5/6 siRNA (5'-CUGGUUUAUGAAACAACUGACAAA CAC-3') (hs.Ri.AGR2.13.8, Integrated DNA Technology). The cells were seeded as previously mentioned; then they were transfected, fixed with 4% PFA after 24/48 h of incubation and processed for immunofluorescence staining. For double transfections, cells were seeded as previously mentioned, transfected with control siRNA or AGR2 exon 2B siRNA, fixed with 4% PFA after two weeks and processed for immunofluorescence staining.

To determine the siRNA-treatment-period that is appropriate to detect a possible early repression of AGR2, before any signs of cell death or reduction in cell densities were observed, cells were seeded and transfected with control siRNA or AGR2 exon 2B siRNA, as previously mentioned. The most appropriate post-transfection incubation periods were then determined to be eight hours for Jed66_GB cells, and 36 h for Jed41_GB. The fixation process and immunofluorescence staining were then carried out in the manner described previously.

siRNA transfections combined with drug treatments

For combined transfections and drug treatments, cells were incubated in 96-well plates in 200 μ L of TM/well at 5×10^3 or 1×10^4 cells/well for Jed66_GB and Jed41_GB, respectively. Cells were either exposed to TM, or transfected with AGR2 exon 2B siRNA as mentioned above. After 24/48 h, the TM was removed, and either DMSO (1%), temozolomide (IC₅₀ at 700 μ M for Jed66_GB and 1000 μ M for Jed41_GB) or irinotecan (IC₅₀ at 2.05 μ M for Jed66_GB and 100 μ M for Jed41_GB) were added. After three days, the cells were fixed and stained using 1% crystal violet with 10% acetic acid, then the absorbance was measured at 595 nm. The combined transfection and drug treatments were also carried out in chamber slides in parallel to assess AGR2 expression via immunofluorescence staining.

Assessment of AGR2 repression and cell densities

To assess cell density, the number of nuclei per 3.9 mm² was counted using ImageJ. The average number of untreated cells per 3.9 mm² was considered as a cell density of 100% and served to calculate the cell density percentage for the average number of treated cells per 3.9 mm².

To assess AGR2 repression in individual cells that were immunofluorescence-co-stained for anti-AGR2 and anti-GRP78, images were analysed using ImageJ. Individual cells were selected using the polygon selection tool, and data for mean area intensities were recorded using the analyse, histogram and RGB tools. At least 100 cells were counted. P53 nuclear expression was assessed in at least 100 cells. All assays were performed in triplicates.

Statistical analysis of the data

The results were analysed using SPSS version 21.0. T-test, Z-test or χ^2 test were used to assess for significant differences in the mean percentage of cell density, survival fractions, areas' intensities and the presence of multinucleated cells.

Results

Basic characteristics of the AGR2-expressed glioblastoma primary cell lines

The two primary Jed66_GB and Jed41_GB cell lines showed a high expression of AGR2, which was detected in both the nucleus and the cytoplasm (Additional file 2: Figure S2A). The primary cell lines had high proliferation rates in culture (doubling times of 5 ± 1.3 days and 8 ± 1.9 days, respectively) and had the ability to form clones (1000 cells initiated an average of 126 clones for Jed66_GB and 43 clones for Jed41_GB after two to three weeks of incubation) (Additional file 2: Figure S2B, C). Both cell lines had medium positive staining for the proliferation marker Ki67 (an average of $47.9 \pm 7.9\%$ and $15.5 \pm 4.7\%$, respectively) and a high positive staining for the cancer biomarker BMI1 (an average of 82.7% and 64.6% , respectively) (Additional file 2: Figure S2D, E). Both cell lines were capable of cell migration as indicated by the scratch assay (Additional file 2: Figure S2F). The cell lines and tissues were whole exome sequenced and rare damaging COSMIC variants present in each cell line and its corresponding tissue (TC) were identified (Additional file 6: Tables S1 and Additional file 7: Table S2). No *IDH*-damaging variants were detected. Two critically damaging variants, the missense variant p.Glu293Lys in the stanniocalcin-2 (*STC2*) gene detected in Jed66_GB and the homozygous missense variant p.Arg273Cys in *TP53* detected in Jed41_GB, were conventionally sequenced, and the results concurred with those detected via whole exome sequencing (Additional file 3: Figure S3A). Neither *AGR2* nor *GRP78* contained critical variants in the cell lines nor in the tissues, and only non-damaging and common variants in these genes were detected (Additional file 3: Figure S3B). The critical functions likely to be affected in the studied cell lines, as per related TC-rare damaging COSMIC variants, are shown in Additional file 8: Table S3. Prominent functions

common to both cell lines are shown in Additional file 3: Figure S3C.

AGR2 colocalises with the UPR marker GRP78 in glioblastoma tissues and corresponding primary cell lines

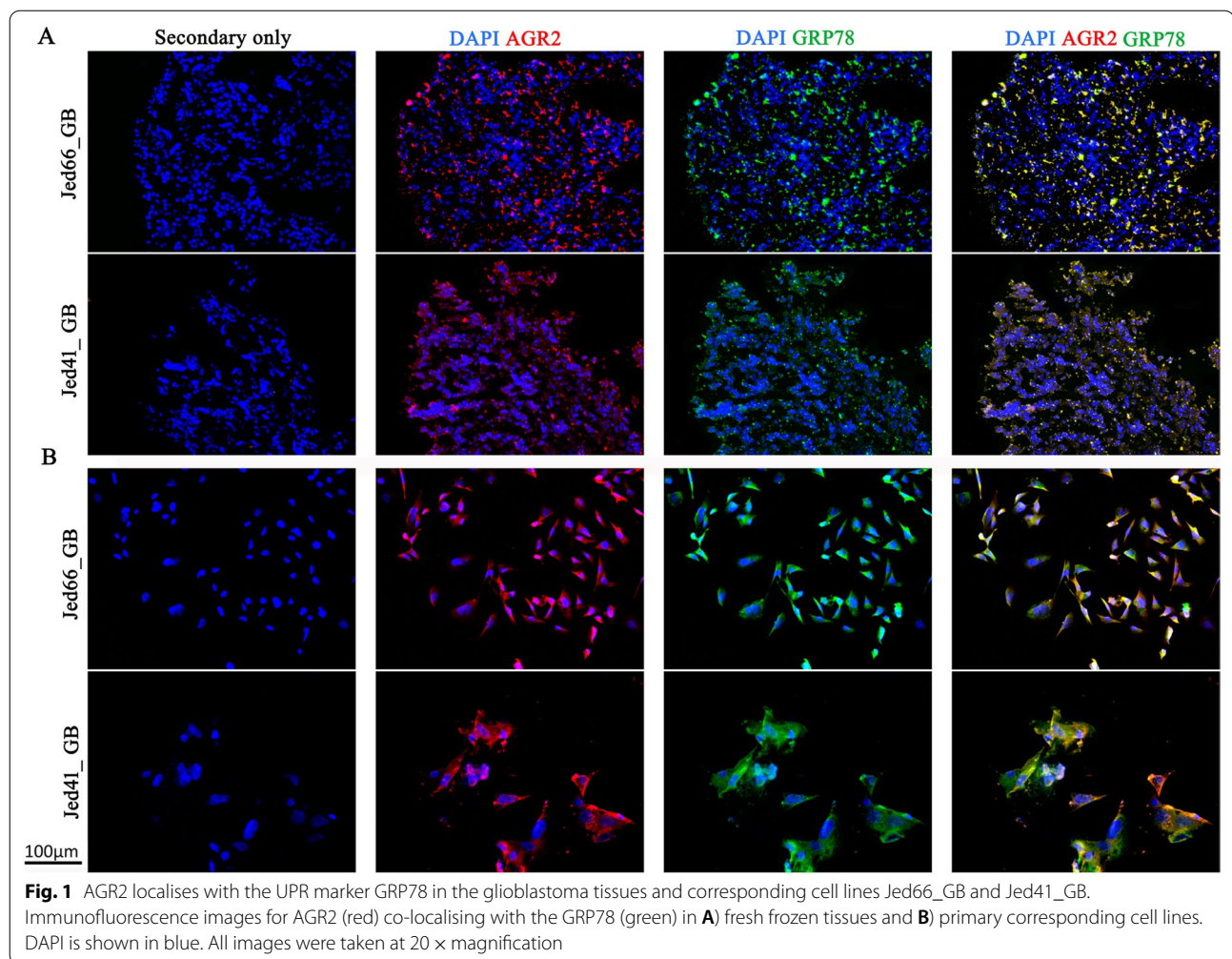
To ensure that the detected expression of AGR2 in both cell lines was not a superficial phenomenon related to cell culturing, the corresponding tissues that were used to generate the primary cell lines were also stained to detect AGR2. Almost all cells in the tissues expressed AGR2 (Fig. 1). To investigate whether AGR2 was co-expressed with its associated partner, the UPR marker GRP78 in the studied samples, AGR2 and GRP78 staining was examined in both tissues and the corresponding cell lines (Fig. 1A and B). The images reveal that AGR2 and GRP78 colocalise in both tissues and cell lines.

AGR2 and GRP78 are highly expressed in glioblastoma CSCs

To investigate the expression of AGR2 and GRP78 in glioblastoma CSCs detected in tissues and corresponding cell lines, AGR2 was co-stained with Nestin, SSEA4 or Vimentin, and GRP78 was co-stained with SOX2, Frizzled 9 and TUBB3 (Fig. 2). All cells that expressed either AGR2 or GRP78 stained positive for several CSC markers. In both cell lines, Nestin, SSEA4, Vimentin, and TUBB3, were highly expressed (percentages ranged between 78.9 and 94.6%), while Frizzled 9 had a high/medium expression (an average of 91.7% in Jed66_GB and an average of 46.3% in Jed41_GB), and SOX2 had a medium/low expression (an average of 44.2% in Jed66_GB and an average of 17.7% in Jed41_GB). Additional markers, including CD133, GFAP and OLIG2, were also co-detected with the UPR proteins (Additional file 4: Figure S4).

AGR2 remains expressed following drug treatment

To assess whether the expression of AGR2 remained high following drug treatment of Jed66_GB and Jed41_GB, both cell lines were drug-treated with a range of clinically applied drugs (Fig. 3). A clonogenic assay was used to observe the ability of cells to form clones following exposure to taxol, irinotecan, cisplatin, MKC8866 and etoposide. A comparison of the clonogenic IC_{50} revealed that both Jed66_GB and Jed41_GB showed high sensitivity to taxol and irinotecan (Taxol IC_{50} 42 μ M and 2 nM, respectively; irinotecan IC_{50} 81 nM and 210 nM, respectively). The sensitivity to cisplatin and MKC8866 for Jed66_GB and Jed41_GB were similar (cisplatin IC_{50} 4 μ M and 12 μ M, respectively; MKC8866 IC_{50} 7.4 μ M and 6.7 μ M, respectively). The least effective applied drug was etoposide (IC_{50} 14 μ M for Jed66_GB and 29 μ M for Jed41_GB).

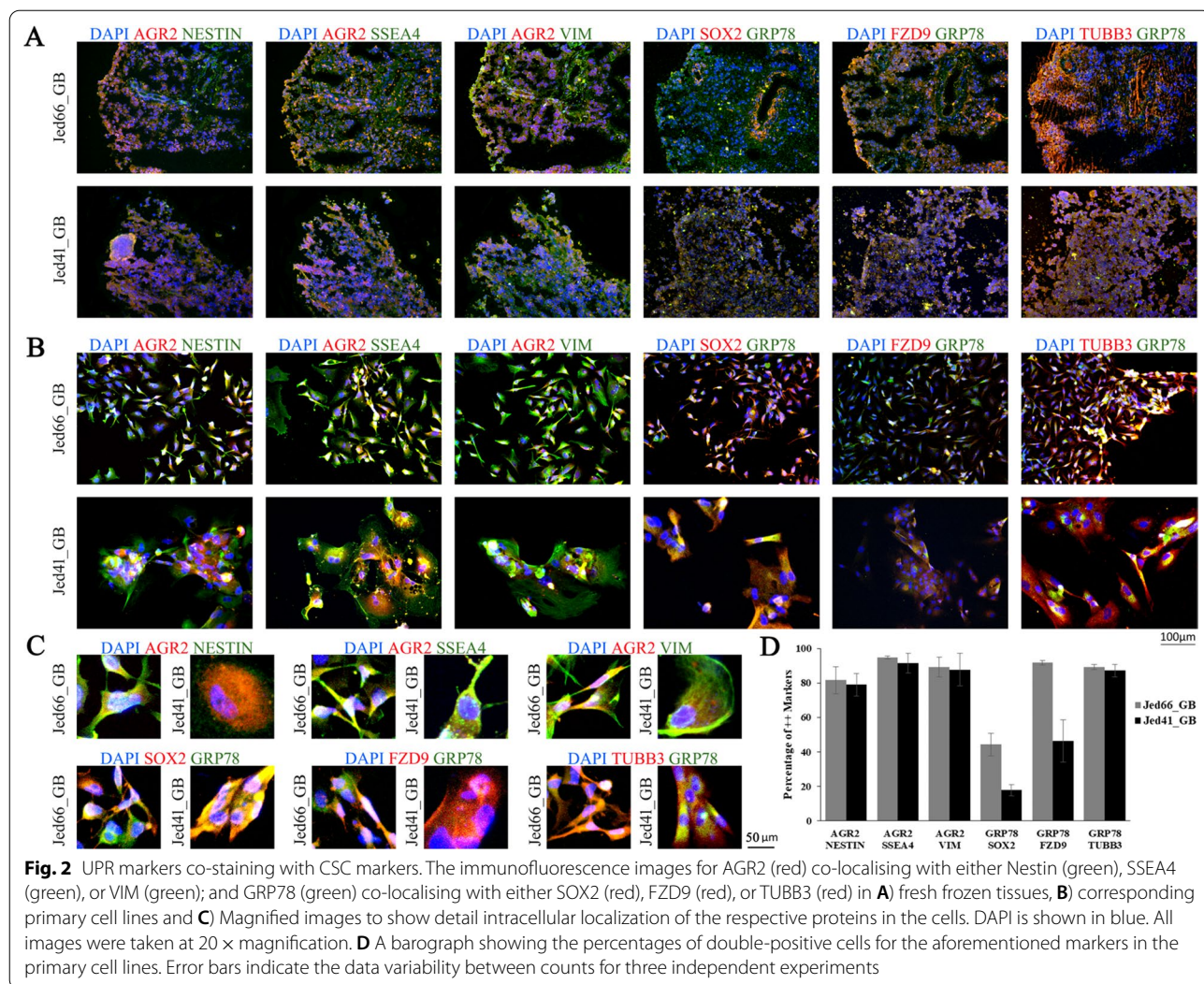


The overall responses to taxol, cisplatin or irinotecan were significantly higher in Jed66_GB than in Jed41_GB ($\text{Chi}^2 = 79.046$, $p < 0.001$, $\text{Chi}^2 = 36.91$, $p < 0.001$, $\text{Chi}^2 = 31.879$, $p < 0.001$, respectively). Critically, the level of expression for AGR2 in both cell lines remained high in resistant surviving cells following the treatments with all drugs at IC_{50} concentrations (Fig. 3C).

AGR2 exon 2B siRNA treatment repressed AGR2 protein expression and led to lower cell-densities in both cell lines

To address whether the presence of AGR2 was essential for cell survival, RNAi-mediated AGR2 repression was applied to both cell lines. Cells were transfected with different concentrations of lipofectamine, and Cy3 and the negative control were used to optimise transfection rates (Additional file 5: Figure S5). Both cell lines were sensitive to the transfection reagents; thus, the maximum possible transfection rate that could be achieved while minimising cell death was approximately 50%.

Three different regions of the gene were targeted with siRNA against exons 2 and 5/6. Clear inhibition of AGR2 expression was seen by immunofluorescence only when targeting exon 2B (Fig. 4A). Within 24/48 h of transfection, targeting exon 2B resulted in a significant reduction of the mean percentages of cell-densities compared with the controls (Fig. 4B). To investigate whether the remaining surviving cells following the first repression could be further AGR2-repressed, cells were treated with AGR2 exon 2B siRNA a second time, as illustrated in Fig. 4C i. Further repression of AGR2 was seen in Figure C ii, and cell densities were adversely affected in both cell lines compared to those exposed to the negative control and Cy3 (Fig. 4C iii). In addition, cell densities were significantly reduced compared with the first repression hit (Fig. 4C iv). However, at least 20% of the cells remained alive and were AGR2-expressed.



Effects of AGR2 exon 2B siRNA treatment in combination with temozolomide or irinotecan

To address the effects of AGR2 exon 2B siRNA treatment in conjunction with the clinically relevant drugs temozolomide and irinotecan, the survival fraction of both cell lines was assessed following single or combination treatments of growth inhibition and siRNA (Fig. 5). For Jed66_GB, AGR2 exon 2B siRNA treatment alone was

significantly more effective than single treatment with either drug (AGR2 exon 2B siRNA versus temozolomide, T-test $p < 0.05$, AGR2 exon 2B siRNA versus irinotecan, T-test $p < 0.05$). Exposure to either drug in combination with siRNA treatment had similar effects when using only siRNA treatment. For Jed41_GB, compared to the control, AGR2 exon 2B siRNA treatment was as effective as a single treatment with either drug. Exposure to

(See figure on next page.)

Fig. 3 AGR2 expression in drug-exposed surviving cells. **A** A schematic diagram showing the timing of AGR2 detection following drug treatment. **B** Clonogenic growth evaluations of the primary cell lines treated with taxol, irinotecan, cisplatin, MKC8866 or etoposide. Error bars represent errors between counts for three independent experiments. Passage numbers for both cell lines ranged from 17 to 33. Three asterisks indicate significant difference at $p < 0.001$. **C** Immunofluorescence images for treated cells at IC_{50} values for the tested drugs. The Jed66_GB cell line was treated with taxol (42pM), irinotecan (81 nM), cisplatin (4 μM), MKC8866 (7.4 μM) or etoposide (14 μM). The Jed41_GB cell line was treated with taxol (2 nM), irinotecan (210 nM), cisplatin (12 μM), MKC8866 (6.7 μM) or etoposide (29 μM). AGR2 is shown in red and DAPI in blue. All images were taken at 20 × magnification

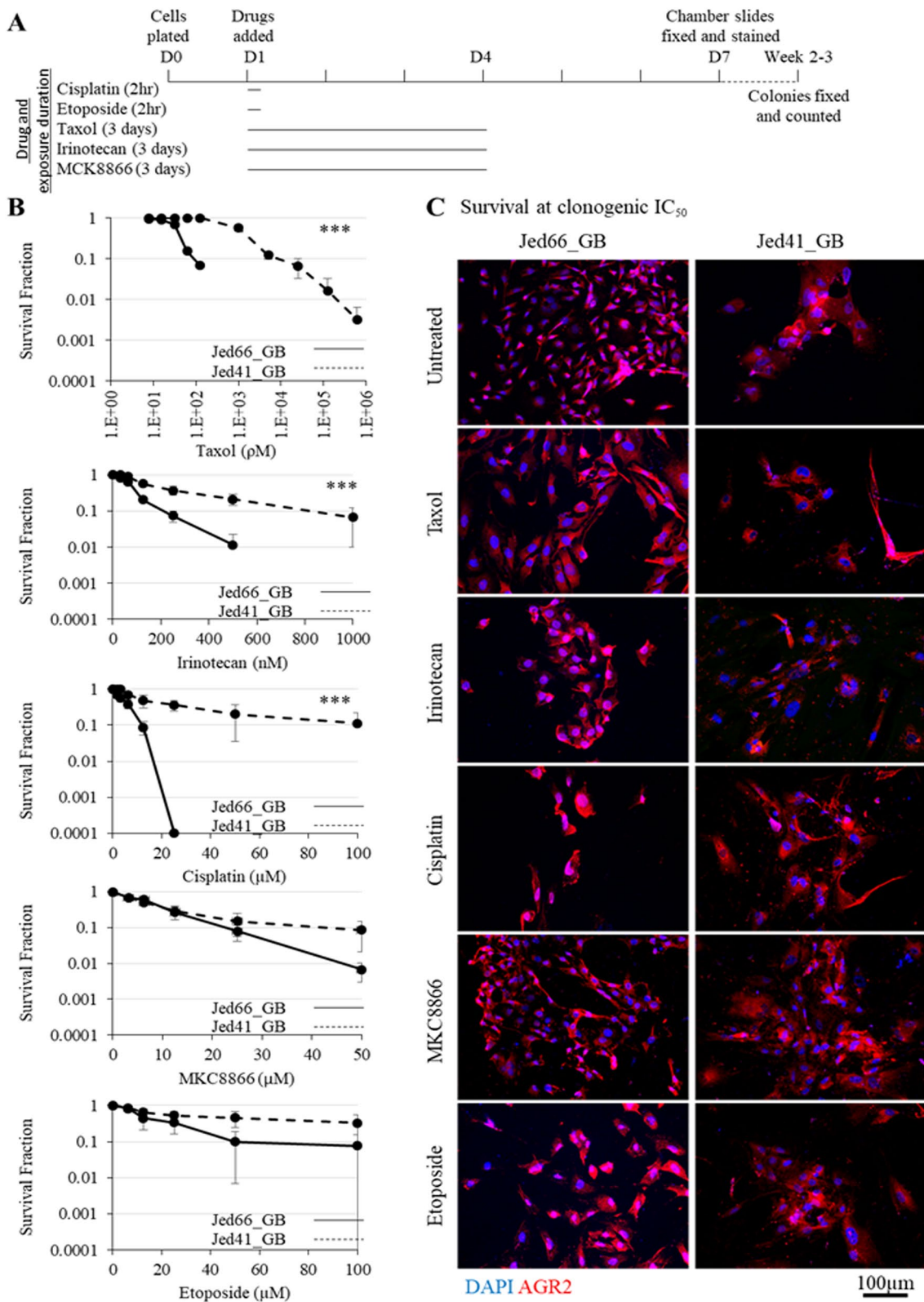
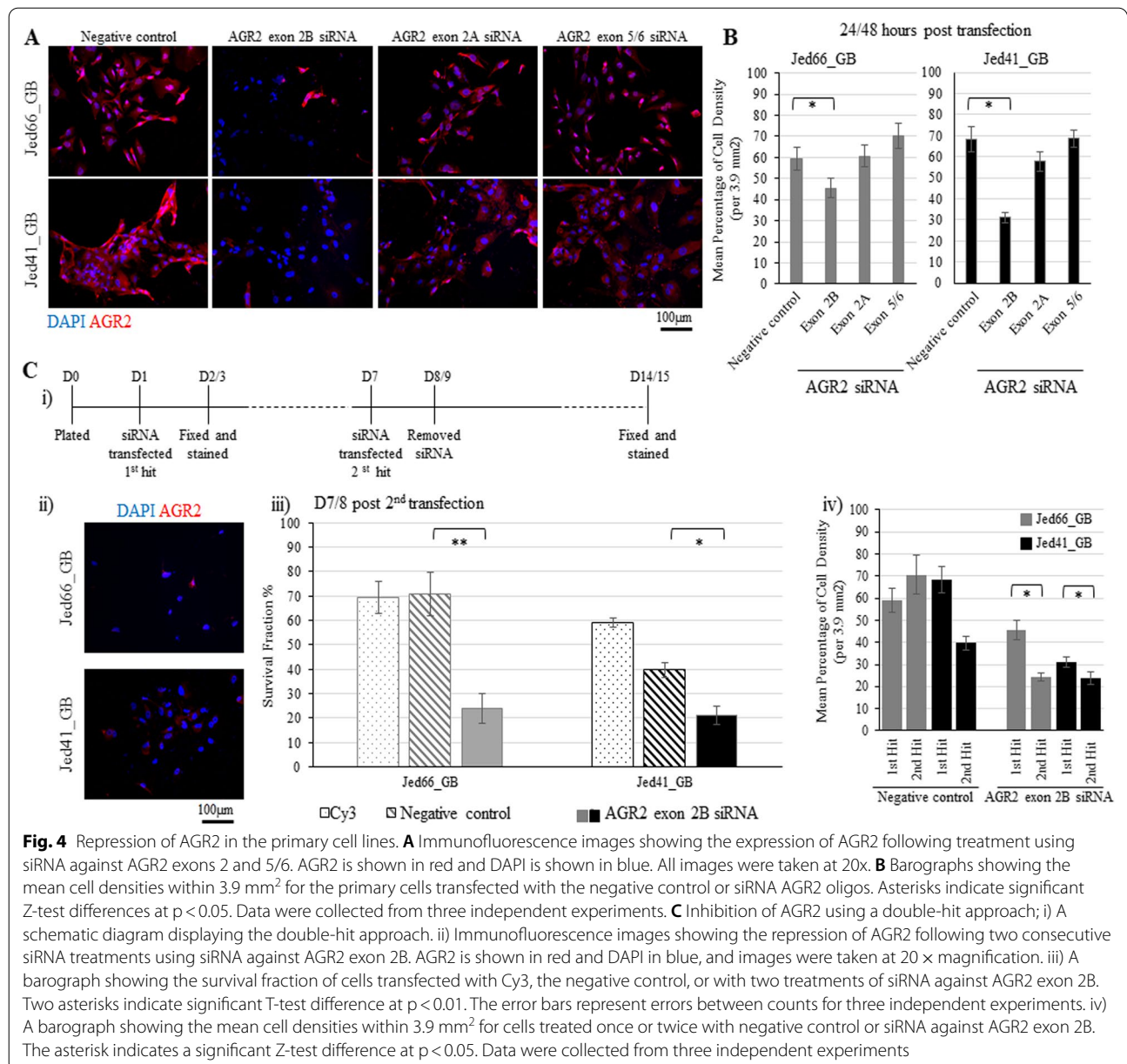


Fig. 3 (See legend on previous page.)

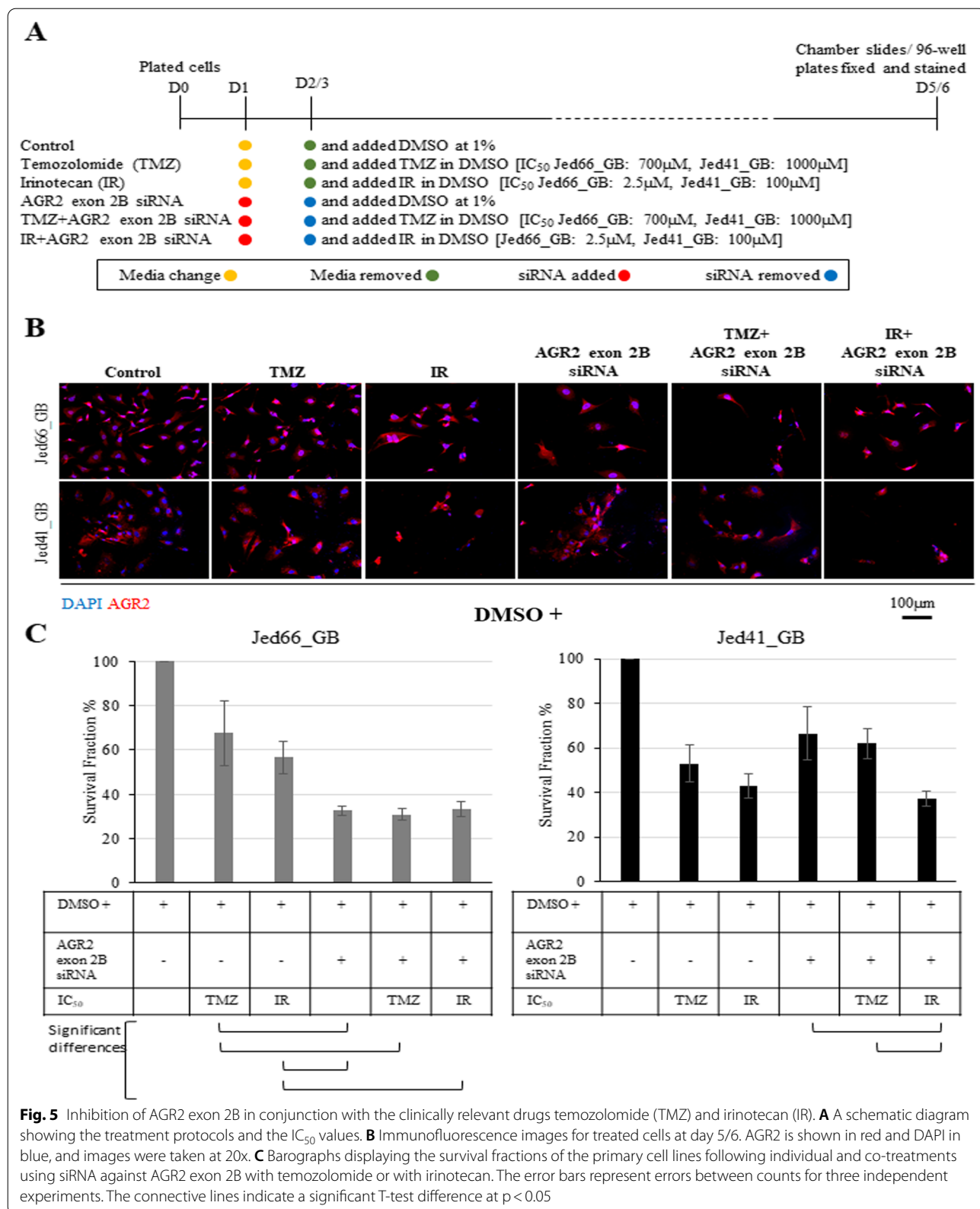


irinotecan in combination with siRNA treatment was the most effective treatment and was significantly more effective than using temozolomide with siRNA (T-test: p < 0.05).

Early repression of AGR2 has cell line-dependent effects

To understand how AGR2 repression may result in the reduction of cell densities or cell death, cells were treated with either negative control siRNA or AGR2 exon 2B siRNA and then analysed following the shortest possible post-transfection periods determined for both cell lines (Fig. 6). A minor reduction of AGR2 expression was

detected in Jed66_GB following eight hours of incubation after transfection, and, in Jed41_GB, following 36 h of incubation after transfection (Fig. 6A). An analysis of single-cell intensities indicated a strong correlation between the expression of AGR2 and GRP78 in control and AGR2 exon 2B siRNA-treated cells, and a reduction of GRP78 expression was seen upon repressing AGR2 (Fig. 6B). In addition, Caspase-3 staining indicated that nuclear expression was significantly increased in both cell lines following AGR2 exon 2B siRNA transfection compared to the negative control siRNA transfection (percentages of Caspase-3 positive cells, Jed66_GB negative



control: $9.48 \pm 3.29\%$, AGR2 exon 2B: $38.35 \pm 6.03\%$, T-test $p < 0.01$; Jed41_GB negative control: $2.06 \pm 0.63\%$, AGR2 exon 2B: $6.89 \pm 2.6\%$, T-test: $p < 0.05$), (Fig. 6C). However, Jed66_GB had a significantly higher nuclear Caspase-3 staining than Jed41_GB in both the negative control siRNA and AGR2 exon 2B siRNA transfected cells (T-test: $p < 0.05$ and T-test: $p < 0.01$, respectively). Critically, the slight repression of AGR2 resulted in the appearance of multinucleation in Jed66_GB, but not in Jed41_GB (Fig. 6D).

Since we detected the presence of damaging variants in *P53* in Jed41_GB but not in Jed66_GB, and since *P53* has a critical role in driving apoptosis, we investigated the presence of nuclear *P53* in glioblastoma cells. The presence of nuclear *P53* was significantly higher in Jed66_GB compared with Jed41_GB in both the negative control siRNA and AGR2 exon 2B siRNA transfected cells ($p < 0.001$) (Fig. 6E).

Discussion

This study focused on understanding the importance of the metastatic-related biomarker AGR2 and the UPR protein GRP78 in glioblastoma tissues and corresponding primary cell lines, with particular attention paid to CSCs and drug resistance. We determined the levels of AGR2 protein expression in recurrent glioblastoma tissues and primary cell lines and showed its co-expression with GRP78 and several CSC markers. We investigated the relationship between AGR2 expression and drug resistance for classically known chemotherapeutics and assessed the effects on cell survival following the repression of AGR2 using siRNA, in combination with chemotherapeutic drugs. In addition, we analysed the early effects of repressing AGR2 and proposed a likely mode of action (Fig. 6F).

Some studies have previously analysed the role of AGR2 or GRP78 in standard glioblastoma cell lines [31, 41]. In our research, we utilised two primary glioblastoma cell lines, adult Jed66_GB and paediatric Jed41_GB,

as primary cell lines represent the ‘central dogma’ of patients’ tumours more accurately than commercially available cell lines [42]. The limitation of using such cell lines is the availability of primary cell lines that are highly adapted to in vitro conditions, can be maintained at relatively low passages and can be harvested for experimentations in sufficient cell numbers. Both Jed66_GB and Jed41_GB were able to grow fast to enable investigations to be carried out in cell passages below 35. Both cell lines were able to form clones and had a high percentage of Ki67- and BMI-positive cells. In addition, both cell lines indicated a high degree of migration in the scratch assay. A whole exome sequencing for Jed66_GB indicated the presence of TC-rare damaging COSMIC variants detected in genes that were previously associated with glioblastoma including BCR activator of RhoGEF and GTPase (*BCR*) [43, 44], TNF receptor associated protein 1 (*TRAP1*) [45–47], DNA polymerase delta 1, catalytic subunit (*POLD1*) [48], otopetrin 1 (*OTOP1*) [49], tyrosine kinase 2 (*TYK2*) [50], AT-rich interaction domain 1B (*ARID1B*) [51], CD48 molecule (*CD48*) [52], ubiquitin specific peptidase 18 (*USP18*) [53], nuclear receptor corepressor 1 (*NCOR1*) [54], NFE2 Like BZIP Transcription Factor 2 (*NFE2L2*) [55], and Kinesin Family Member 1A (*KIF1A*) [56]. For Jed41_GB, exome sequencing showed the presence of TC-rare damaging COSMIC variants detected in glioblastoma-associated genes including *TP53* [43, 44, 57], LDL receptor related protein 1B (*LRP1B*) [44, 58], adhesion G protein-coupled receptor E5 (*ADGRE5*) [59], atrophin 1 (*ATNI*) [60], autophagy related 2B (*ATG2B*) [61, 62], MYC associated zinc finger protein (*MAZ*) [23, 63], WNK lysine deficient protein kinase 1 (*WNK1*) [64, 65], UDP glucuronosyltransferase family 1 member A1 (*UGT1A1*) [66], and UDP glucuronosyltransferase family 1 member A6 (*UGT1A6*) [67]. Not surprisingly, differences in functional characteristics between the two cell lines were demonstrated, consistent with the high inter-patient heterogeneity seen for glioblastoma [6–9, 15].

(See figure on next page.)

Fig. 6 The effects of early repression of AGR2 in both Jed66_GB and Jed41_GB. **A** i) Images showing minor repression of AGR2 in both cell lines following the short post-transfection of eight hours for Jed66_GB and 36 h for Jed41_GB. ii) The AGR2 mean intensities for negative control and AGR2 exon 2B siRNA-transfected cells. The asterisk indicates significant T-test difference at $p < 0.05$. **B** GRP78 expression and AGR2 expression in both negative control and AGR2 exon 2B siRNA-transfected cells for both cell lines. **C** Immunofluorescence images of nuclear Caspase-3 in negative control and AGR2 exon 2B siRNA-transfected cells. The arrow points to a Caspase-3-positive multinucleated cell. Caspase-3 is shown in red and DAPI in blue. **D** i) Images show multinucleation in Jed66_GB ii) The percentage of multinucleated cells in Jed66_GB following negative control and AGR2 exon 2B siRNA transfections. Asterisk indicate T-test significant difference at $p < 0.05$. **E** i) Immunofluorescence images displaying the expression of *P53* in both cell lines following negative control and AGR2 exon 2B siRNA transfections. *P53* is shown in green and DAPI in blue. ii) Magnified images showing *P53* localisation. iii) The percentage of cells positive for nuclear *P53* was significantly higher in Jed66_GB compared with Jed41_GB. Three asterisks indicate T-test significant difference at $p < 0.001$. **F** A suggested model that explains the role of AGR2 in glioblastoma. Both in situ and in vitro, AGR2 and GRP78 are highly expressed in CSCs and drug-resistant cells. Upon repression of AGR2, GRP78 was also reduced. Early cell fate seems to be dependent on the used model, and can lead either to multinucleation followed by cell death or to delayed growth followed by attenuated cell death

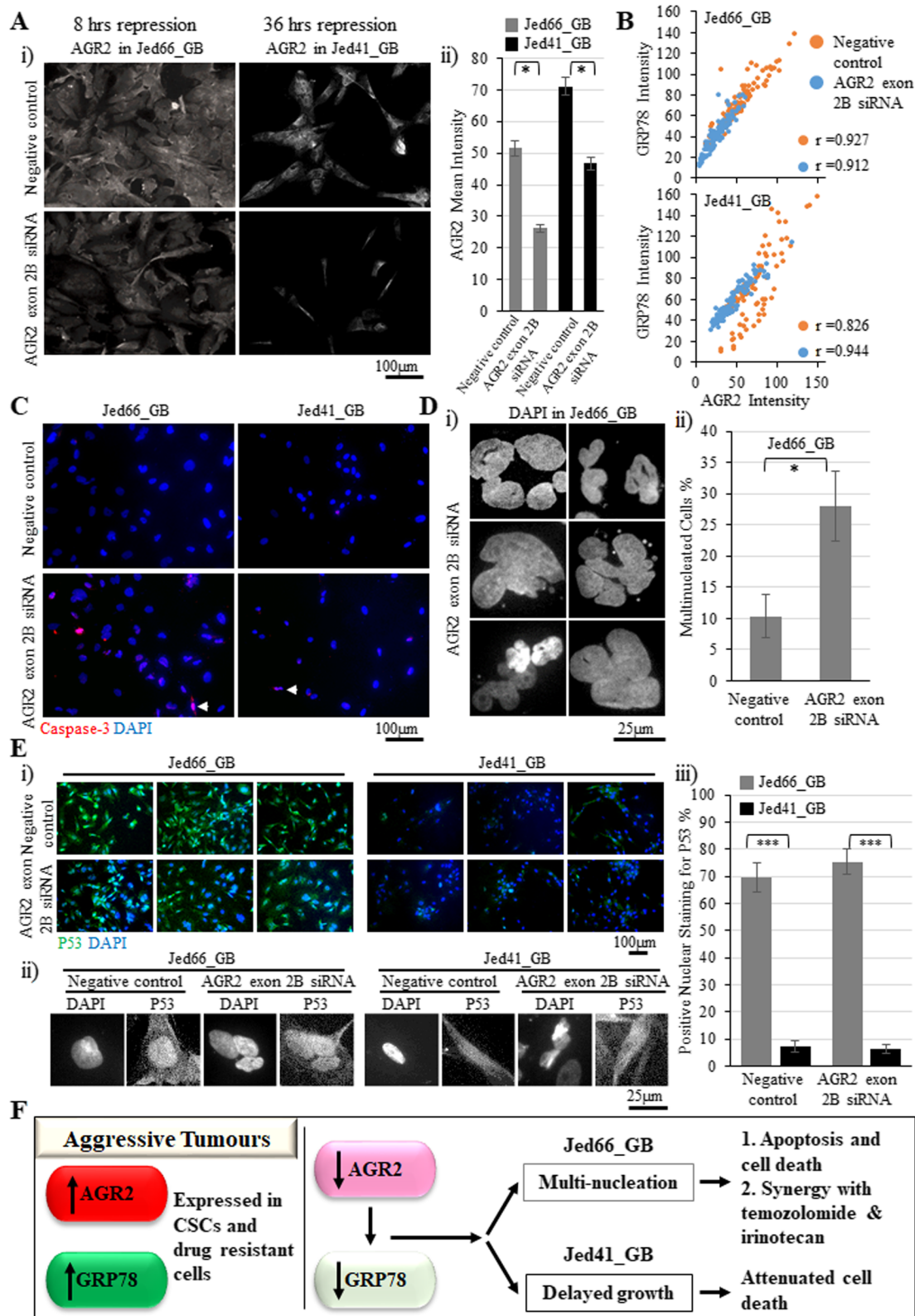


Fig. 6 (See legend on previous page.)

Immunofluorescence results showed, for the first time, a clear subcellular co-localisation for AGR2 with GRP78 in glioblastoma in situ and in the corresponding cell lines. This is consistent with the notion that AGR2 is an interacting partner of GRP78 [17, 24]. In addition, both proteins had an elevated expression, a phenomenon previously detected in glioblastoma [19, 32, 68]. Notably, AGR2 is not expressed in normal brain tissues [26], and it was shown to be preferentially expressed in high grade meningiomas compared to low grade meningiomas [39]. AGR2 overexpression has been linked to higher ER stress [69, 70], possibly via several modulators [17, 32]. Surprisingly, AGR2 was detected in the nucleus in both cell lines, a unique feature that was not seen in situ, suggesting that AGR2 behaviour is likely to be responsive to the tumour microenvironment [71, 72].

CSCs are well identified in glioblastoma [7, 9], and several associated markers have been studied [13, 14]. The finding that both AGR2 and GRP78 proteins are colocalised with CSC markers in the same tissues as well as in the corresponding cell lines suggests a functional interaction of AGR2 and GRP78 in glioblastoma-CSCs. Several studies have shown an indirect correlation between the expression of either protein and CSCs markers [20, 31]. The high expression of AGR2 has been previously associated with the expression of Nestin, CD133 and SOX2 in high-grade meningioma tissues [39]. AGR2 expression was also shown to have a strong positive correlation with nanog homeobox (NANOG) in oral squamous cell carcinoma [73]. The effect of high GRP78 expression in glioblastoma-CSCs is still being investigated. A previous study demonstrated that using the ER stressor drug thapsigargin resulted in the increased expression of GRP78, and the reduced expression of SOX2 in glioblastoma patient derived CSCs [20]. However, in that work, SOX2 downregulation was not shown to be directly affected by the UPR pathway. The data presented here show the co-presence of GRP78 in cells expressing SOX2, FZD9, OLIG2, GFAP or TUBB3, suggesting that the presence of GRP78 does not directly inhibit the aforementioned CSC markers. In addition, similar to other studies, Ki67 expression was seen in a few cells that express GRP78 [74, 75], indicating that proliferation is not inhibited in UPR-active CSCs.

The expression of AGR2 remained high in drug-resistant cells following treatments with a range of clinically applied drugs that utilize different modes of action [76–80]. This suggests that the presence of AGR2 is critical for glioblastoma cell survival, regardless of drug type. Interestingly, of all the applied drugs, the primary cell lines were most sensitive to taxol, an observation previously noted in glioblastoma-standard cell lines [81, 82]. The endoplasmic reticulum to nucleus signalling 1 (ERN1),

otherwise known as bifunctional endoribonuclease/protein kinase (IRE1), is a UPR activator and has been suggested as an influential regulator of AGR2 [17]. The ERN1 inhibitor, MKC8866, was less effective in inhibiting clone formations than irinotecan or taxol; however MKC8866 was similarly effective in both cell lines, suggesting that the UPR machinery is equally active in the studied cell lines.

Short and prolonged RNAi-mediated AGR2 exon 2B repression led to lower cell densities in both cell lines. Exon 2 covers nucleotides 66–211 and its transcript is thought to be present in the AGR2 full lengths, AGR2vC and AGR2vH isoforms [25]. In this study, two siRNAs were used to target exon 2; however, only AGR2 exon 2B siRNA, effecting a region that codes for amino acids 33–40 AA (TKDSRPKL), was detrimental. Previously, repression of AGR2 via targeting exon 7 or exon 8 in glioblastoma standard cell lines showed disruptions in the cell cycle, cell growth, migration, and cell invasion [41, 83, 84]. In colorectal cancer cells, AGR2 exon 2 knockout was shown to be crucial for protein-mediated cell adhesion, and resulted in the increase of reaction oxygen species production [85]. This suggests that targeting different regions of AGR2 results in different responses that may also be cell line dependent.

Knocking down AGR2 using siRNA against AGR2 exon 2B in the primary cell lines had partially synergistic effects with the glioblastoma-associated drugs temozolomide and irinotecan. AGR2 knockout, in combination with other drugs, was previously shown to be effective in inhibiting the growth of different cell line models [85–88]. To the best of our knowledge, this is the first study to show observations related to the effect of siRNA against AGR2 exon 2 in combination with either temozolomide or irinotecan. Inhibiting AGR2 exon 2B was significantly more effective than a single treatment with either drug in Jed66_GB, and exposure to either drug with siRNA did not affect the survival fraction that was achieved when using siRNA only. However, this was not necessarily the case for Jed41_GB. This is consistent with the notion that heterogeneity in glioblastoma patients has an impact on drug response [8, 9]. Thus, although inhibiting AGR2 exon 2B may be therapeutically effective, a preselection of sensitive tumours is likely to be necessary. Further work is needed to decipher the exact mechanism of action for the interplay between AGR2 inhibition and the aforementioned drugs.

How the repression of AGR2 could lead to the reduction of cell densities or cell death was partially clarified when observations for the earliest time points of repression were made for Jed66_GB and Jed41_GB (8 h and 36 h, respectively). Both cell lines increased nuclear Caspase-3 activation following a slight reduction in AGR2,

a feature seen previously in primary breast cancer cells [87]. However, the early effects seen following repression were different between the two cell lines. First, Jed66_GB had a higher capacity to activate nuclear Caspase-3 than Jed41_GB in the controls and repressed cells. This is perhaps due to the presence of wild-type *P53* in Jed66_GB compared with mutated *P53* in Jed41_GB. This is also consistent with the observations that Jed41_GB is more resistant to taxol, cisplatin and irinotecan compared with Jed66_GB. However, the higher capacity of Jed66_GB to proliferate could contribute to better overall recovery following treatment.

Second, early repression of AGR2 led to multinucleation only in Jed66_GB. This indicates that the pathway to induce apoptosis following AGR2 repression is cell line-dependent. How can the repression of AGR2 lead to apoptosis via multiple pathways? It was previously known that AGR2 can affect the presence of multiple molecules [17, 86, 89, 90]. This global impact of AGR2 is likely to occur via modulating the ER degradation enhancing, alpha-mannosidase-like protein 1 (EDEM), which is a critical component in the ERAD system [17, 83]. One can postulate that in a system similar to Jed66_GB, where proliferation is high, and defects in genes such as *PLOD1* that are associated with nuclear integrity exist [91], the repression of AGR2 could then interfere with the cytoskeleton, via increasing the degradation of β -dystroglycan [92], which is a basement membrane component required to bind to actin and is critical for the integrity of the cytoskeleton [93]. Alternatively, in a cell line with wild-type *p53*, where the threshold of nuclear integrity is dependent on a functional *P53*, repression of AGR2 may interfere with *P53*, as previously shown, and cause multinucleation [94, 95]. In contrast, in a system such as Jed41_GB, where cells grow slower, have adapted to dysfunctional genes that are important for nuclear integrity such as *P53*, leukaemia NUP98 fusion partner 1 (*LNPI*) and Sad1 and UNC84 domain containing 2 (*SUN2*) [96, 97], the repression of AGR2 could then directly induce apoptosis by enabling the degradation of the anti-apoptotic proteins B-cell lymphoma 2 (*Bcl2*) and BCL2 Like 1 (*Bcl2l1*), as previously seen in head and neck squamous cell carcinoma cell lines [98].

Conclusion

In conclusion, the data demonstrate that AGR2 and GRP78 are highly expressed in glioblastoma CSCs and drug-resistant cells in situ and in vitro. The repression of AGR2 exon 2B using siRNA resulted in the reduction of cell densities and was synergistically effective in decreasing cell densities of temozolomide- and irinotecan-treated Jed66_GB cells. The suppression of AGR2 influenced the presence of GRP78, possibly through

navigating the UPR machinery. Early cell fate seemed to depend on the presence of wild-type *P53* and can either lead to multinucleation followed by cell death or to delayed growth followed by attenuated cell death. Further work is critical to investigate the relationship between AGR2 and *P53* and their impact on cell death following drug treatment in a larger cohort.

Abbreviations

ADGRES: Adhesion G protein-coupled receptor E5; AGR2: Anterior gradient homologue 2; AKT3: AKT serine/threonine kinase 3; ARID1B: AT-rich interaction domain 1B; ATG2B: Autophagy related 2B; ATN1: Atrophin 1; Bcl2: B-cell lymphoma 2; Bcl2l1: BCL2 Like 1; BCR: BCR activator of RhoGEF and GTPase; BMI1: BMI1 proto-oncogene, polycomb ring finger; CD133: Prominin 1; CD48: CD48 molecule; CDKN2A: Cyclin dependent kinase inhibitor 2A; CNS: Central nervous system tumours; COSMIC: Catalogue of somatic mutations in cancer; CSCs: Cancer stem cells; CTNBN1: Catenin beta 1; DT: Doubling time; EDEM: Enhancing alpha-mannosidase like protein 1; EGFR: Epidermal growth factor receptor; ER: Endoplasmic reticulum; ERAD: Endoplasmic-reticulum-associated protein degradation; ERN1: Endoplasmic reticulum to nucleus signalling 1; FGFR2: Fibroblast growth factor receptor 2; FZD9: Frizzled class receptor 9; GB: Glioblastoma; GFAP: Glial fibrillary acidic protein; GRP78: Glucose regulatory protein 78/BIP; IRE1: Endoribonuclease/protein kinase; IRS2: Insulin receptor substrate 2; IDH1/2: Isocitrate dehydrogenase (IDH) 1 and 2, KIF1A: kinesin family member 1A; LNP1: Leukaemia NUP98 fusion partner 1; LRP1B: LDL receptor related protein 1B; MAZ: MYC associated zinc finger protein; NANOG: Nanog homeobox; NCOR1: Nuclear receptor corepressor 1; NF1: Neurofibromin 1; NFE2L2: NFE2 Like BZIP transcription factor 2; NOTCH1: Notch receptor 1; NUDCD3: Nucleo domain containing 3; OLIG2: Oligodendrocyte transcription factor 2; OTOPI1: Otopetrin 1; P53: Tumour protein p53; Park2: Parkin RBR E3 ubiquitin protein ligase; PFA: Paraformaldehyde; POLD1: DNA polymerase delta 1, catalytic subunit; PTEN: Phosphatase and tensin homolog; PTPred: Protein tyrosine phosphatase receptor type D; siRNA: Small interfering duplex RNA sequences; SOX2: SRY-Box transcription factor 2; SSEA4: Stage-specific embryonic antigen-4; STC2: Stanniocalcin-2; SUN2: Sad1 and UNC84 domain containing 2; TC: Tissue cell line; TM: Transfection media; TRAP1: TNF receptor associated protein 1; TUBB3: Tubulin beta 3 class III; TYK2: Tyrosine kinase 2; UGT1A1: UDP glucuronosyltransferase family 1 member A1; UGT1A6: UDP glucuronosyltransferase family 1 member A6; UPR: Unfolded protein response; USP18: Ubiquitin specific peptidase 18; VCF: Variant call format; VIM: Vimentin; WES: Whole exome sequencing; WNK1: WNK lysine deficient protein kinase 1.

Supplementary Information

The online version contains supplementary material available at <https://doi.org/10.1186/s12935-022-02814-5>.

Additional file 1: Figure S1. Histopathological classifications. Jed66_GB has malignant glial cells palisade around a central focus of necrosis and microvascular proliferations on the left and right sides (H&E stain; power 200 X). The tumour is positive for GFAP immunostaining (Power 100 X). Jed41_GB has numerous large bizarre multinucleated tumour cells on the right side and tumour necrosis on the left side (H&E stain; power 400 X). The tissue was GFAP positive (Power 100 X).

Additional file 2: Figure S2. Biological characteristics of the glioblastoma primary cell lines Jed66_GB and Jed41_GB. A) Immunofluorescence images showing i) the expression of AGR2, ii) Nuclear localisation of AGR2. AGR2 is shown in red and DAPI in blue. Images were taken at 20x. B) A barograph displaying the doubling time for each cell line. Error bars represent errors between counts for three independent experiments. C) A line graph showing the clonogenic capacity for Jed66_GB cells (Passages 17-23) and Jed41_GB cells (Passages 8-14). Error bars represent errors between counts for three independent experiments. D) Immunofluorescence images showing the expression of Ki67 (red) or BMI (green) in both primary cell lines. Images were taken at 20x. E) A barograph showing the average percentage of cells positive for Ki67 or BMI. The error bars

represent errors between counts for three independent experiments. F) Images of cells that underwent a scratch assay taken on day 0 before and after scratch and at days 3 and 4 after the gap was filled. Images were taken at 5x magnification.

Additional file 3: Figure S3. Sequencing variants in the primary cell lines and corresponding tissues. A) Conventional sequencing for two critically damaging variants present in either cell line with its corresponding tissue, *STC2* in Jed66_GB and *TP53* in Jed41_GB. B) Only non-damaging and common variants for *AGR2* or *GRP78* were detected in either cell line. C) Prominent functions likely to be affected for both cell lines, as per related TC rare damaging COSMIC variants. Prominent functions are coloured in grey, genes affected in Jed66_GB are coloured in blue and those identified in Jed41_GB are coloured in green.

Additional file 4: Figure S4. Further UPR markers co-stained with CSC markers in the primary cell lines. A) Immunofluorescence images for *AGR2* (red) co-stained with *CD133* (green), and *GRP78* (green) co-stained with *GFAP* (red), or with *OLIG2* (Red). DAPI is shown in blue. Images were taken at 20x magnification. B) Magnified images to show detail intracellular localization of the respective proteins. C) A barograph showing the percentages of double-positive cells for the aforementioned markers in the primary cell lines. Error bars represent errors between counts for three independent experiments.

Additional file 5: Figure S5. siRNA optimisation for the primary cell lines. A) Barographs showing the survival fractions for the Cy3 transfection control and siRNA negative control at optimum concentrations of lipofectamine. Error bars represent errors between counts for three independent experiments. B) Immunofluorescence images showing the Cy3-positive cells are shown in red, and DAPI is shown in blue. Images were taken at 20x magnification. C) A barograph showing the percentages of Cy3-positive cells. Error bars represent errors between counts for three independent experiments. D) Immunofluorescence images showing cell densities following transfections, and the images were taken at 5x magnification. Cy3-positive cells are shown in red, and DAPI is shown in blue.

Additional file 6: Table S1. Rare damaging COSMIC variants detected in the tissue and cell lines for Jed66_GB.

Additional file 7: Table S2. Rare damaging COSMIC variants detected in the tissue and cell lines for Jed41_GB.

Additional file 8: Table S3. It is likely affect prominent functions in the studied cell lines. Genes with rare damaging COSMIC variants were detected in the tissue and corresponding cell line for each patient and organized by prominent functions (Panther: Molecular Function/ Biological Process/Pathway/Reactome Pathway, NCBI Gene information*) for both Jed66_GB and Jed41_GB. Only variants with a possible/probable damaging PolyPhen effect were included, as per data annotated by BaseSpace or as detected manually using PolyPhen-2 Wiki.

Acknowledgements

We would like to thank the KFMRRC administration and technical departments for their support in particular M-Zaki Mustafa ElAssouli.

Author contributions

Conceptualisation: DH, RC, HS, SB, MB, FA, MS, AC and AA. Data curation and methodology: DH, RA, AA, RG, AA, and HS. Formal analysis: DH, RA, and HS. Funding acquisition: DH, RC, HS, SB, MB, FA, MS, TZ, AC and AA. Supervision: DH and AAH. Validation: DH, RA and HS. Writing (original draft): DH and RA. Writing (review and editing): DH, RA, AA, RG, AA, AAH, HS, SB, MB, FA, RC, MS, TZ, AC and AA. All authors have read and approved the final manuscript.

Funding

This work was funded by Research & Development Office, Ministry of Education, Kingdom of Saudi Arabia, Collaborative Research Project 222.

Availability of data and materials

The datasets used and/or analysed during the current study are available from the corresponding author on reasonable request.

Declarations

Ethics approval and consent to participate

This work was approved by the Ethical Board of King Abdulaziz University Hospital (board registration no. at the National Committee of Bio- and Medical Ethics: HA-02-J-008; Project reference no. 976–12).

Consent for publication

A signed informed consent form designed according to the Declaration of Helsinki was obtained from the primary relatives.

Competing interests

The authors declare that the research was conducted in the absence of any commercial or financial relationships that could be construed as potential conflicts of interest.

Author details

¹King Fahd Medical Research Center, King Abdulaziz University, 80216, Jeddah 21589, Saudi Arabia. ²Department of Medical Laboratory Sciences, Faculty of Applied Medical Sciences, King Abdulaziz University, Jeddah 21589, Saudi Arabia. ³Department of Biological Sciences, Faculty of Science, King Abdulaziz University, 80203, Jeddah 21589, Saudi Arabia. ⁴College of Health Sciences, Al-Rayan Colleges, 41411, Madinah AL-Munawarah, Saudi Arabia. ⁵Center of Excellence in Genomic Medicine Research, Department of Medical Laboratory Technology, Faculty of Applied Medical Sciences, King Abdulaziz University, Jeddah 21589, Saudi Arabia. ⁶Division of Neurosurgery, Faculty of Medicine, King Abdulaziz University, Jeddah 21589, Saudi Arabia. ⁷Pathology Department, Faculty of Medicine, King Abdulaziz University, Jeddah 21589, Saudi Arabia. ⁸School of Engineering and Sustainable Development, Emerging Technologies Research Centre (EMTERC), De Montfort University, The Gateway, Leicester LE1 9BH, UK. ⁹Centre of Innovation for Personalized Medicine, Department of Medical Laboratory Technology, Faculty of Applied Medical Sciences, King Abdulaziz University, Jeddah 21589, Saudi Arabia.

Received: 12 September 2022 Accepted: 28 November 2022

Published online: 08 December 2022

References

- Wen PY, Packer RJ. The 2021 WHO classification of tumors of the central nervous system: clinical implications. *Neuro Oncol.* 2021;23(8):1215–7.
- Alexopoulos G, Zhang J, Karamelas I, Patel M, Kemp J, Coppens J, Mattei TA, Mercier P. Long-term time series forecasting and updates on survival analysis of glioblastoma multiforme, a 1975–2018 population-based study. *Neuroepidemiology.* 2022;56(2):75–89.
- Cosnarovici MM, Cosnarovici RV, Piciu D. Updates on the 2016 World Health Organization classification of pediatric tumors of the central nervous system—a systematic review. *Med Pharm Rep.* 2021;94(3):282–8.
- Stylli SS. Novel treatment strategies for glioblastoma—a summary. *Cancers.* 2021;13(22):5868–72.
- Weller M, Reifenberger G. Beyond the World Health Organization classification of central nervous system tumors 2016: what are the new developments for gliomas from a clinician's perspective? *Curr Opin Neurol.* 2020;33(6):701–6.
- Darmanis S, Sloan SA, Croote D, Mignardi M, Chernikova S, Samghababi P, Zhang Y, Neff N, Kowarsky M, Caneda C, et al. Single-cell RNA-seq analysis of infiltrating neoplastic cells at the migrating front of human glioblastoma. *Cell Rep.* 2017;21(5):1399–410.
- Patel AP, Tirosh I, Trombetta JJ, Shalek AK, Gillespie SM, Wakimoto H, Cahill DP, Nahed BV, Curry WT, Martuza RL, et al. Single-cell RNA-seq highlights intratumoral heterogeneity in primary glioblastoma. *Science.* 2014;344(6190):1396–401.
- Filbin MG, Tirosh I, Hovestadt V, Shaw ML, Escalante LE, Mathewson ND, Neftel C, Frank N, Pelton K, Hebert CM, et al. Developmental and oncogenic programs in H3K27M gliomas dissected by single-cell RNA-seq. *Science.* 2018;360(6386):331–5.
- Neftel C, Laffy J, Filbin MG, Hara T, Shore ME, Rahme GJ, Richman AR, Silverbush D, Shaw ML, Hebert CM, et al. An integrative model of cellular

- states, plasticity, and genetics for glioblastoma. *Cell*. 2019;178(4):835–849 e821.
10. Malta TM, de Souza CF, Sabetod TS, Silva TC, Mosella MS, Kalkanis SN, Snyder J, Castro AVB, Noushmehr H. Glioma CpG island methylator phenotype (G-CIMP): biological and clinical implications. *Neuro Oncol*. 2018;20(5):608–20.
 11. Walcher L, Kistenmacher AK, Suo H, Kitte R, Dluczek S, Strauss A, Blaudszun AR, Yeysa T, Fricke S, Kossatz-Boehlert U. Cancer stem cells—origins and biomarkers: perspectives for targeted personalized therapies. *Front Immunol*. 2020;11:1280–312.
 12. Hanahan D. Hallmarks of cancer: new dimensions. *Cancer Discov*. 2022;12(1):31–46.
 13. Herrera-Oropeza GE, Angulo-Rojo C, Gastelum-Lopez SA, Varela-Echavarría A, Hernandez-Rosales M, Avina-Padilla K. Glioblastoma multiforme: a multi-omics analysis of driver genes and tumour heterogeneity. *Interface Focus*. 2021;11(4):20200072–93.
 14. Khan IN, Ullah N, Hussein D, Saini KS. Current and emerging biomarkers in tumors of the central nervous system: possible diagnostic, prognostic and therapeutic applications. *Semin Cancer Biol*. 2018;52(Pt 1):85–102.
 15. Alamir H, Alomari M, Salwati AAA, Saka M, Bangash M, Baeesa S, Alghamdi F, Carracedo A, Schulten HJ, Chaudhary A, et al. In situ characterization of stem cells-like biomarkers in meningiomas. *Cancer Cell Int*. 2018;18:77–90.
 16. Radanovic T, Ernst R. The unfolded protein response as a guardian of the secretory pathway. *Cells*. 2021;10(11):2965–87.
 17. Alserihi R, Schulten HJ, Bakhashab S, Saini K, Al-Hejin AM, Hussein D. Leveraging the role of the metastatic associated protein anterior gradient homologue 2 in unfolded protein degradation: a novel therapeutic biomarker for cancer. *Cancers*. 2019;11(7):890–917.
 18. Wang L, Zhang Y, Wang W, Zhu Y, Chen Y, Tian B. Gemcitabine treatment induces endoplasmic reticular (ER) stress and subsequently upregulates urokinase plasminogen activator (uPA) to block mitochondrial-dependent apoptosis in Panc-1 cancer stem-like cells (CSCs). *PLoS ONE*. 2017;12(8):e0184110.
 19. Yang S, Lu H, Luo F, Zhang Z, Wu W. Increased expression of GRP78 correlates with adverse outcome in recurrent glioblastoma multiforme patients. *Turk Neurosurg*. 2020;30(1):557–64.
 20. Penaranda-Fajardo NM, Meijer C, Liang Y, Dijkstra BM, Aguirre-Gamboa R, den Dunnen WFA, Kruyt FAE. ER stress and UPR activation in glioblastoma: identification of a noncanonical PERK mechanism regulating GBM stem cells through SOX2 modulation. *Cell Death Dis*. 2019;10(10):690–705.
 21. Chen Z, Wang H, Zhang Z, Xu J, Qi Y, Xue H, Gao Z, Zhao R, Wang S, Zhang S, et al. Cell surface GRP78 regulates BACE2 via lysosome-dependent manner to maintain mesenchymal phenotype of glioma stem cells. *J Exp Clin Cancer Res*. 2021;40(1):20–36.
 22. Liu G, Yu J, Wu R, Shi L, Zhang X, Zhang W, Zhong X, Wang Y, Li H, Shen Y, et al. GRP78 determines glioblastoma sensitivity to UBA1 inhibition-induced UPR signaling and cell death. *Cell Death Dis*. 2021;12(8):733–45.
 23. Luo W, Zhu X, Liu W, Ren Y, Bei C, Qin L, Miao X, Tang F, Tang G, Tan S. MYC associated zinc finger protein promotes the invasion and metastasis of hepatocellular carcinoma by inducing epithelial mesenchymal transition. *Oncotarget*. 2016;7(52):86420–32.
 24. Bouchalova P, Sommerova L, Potesil D, Martisova A, Lapcik P, Koci V, Scherl A, Vonka P, Planas-Iglesias J, Chevet E, et al. Characterization of the AGR2 interactome uncovers new players of protein disulfide isomerase network in cancer cells. *Molecular Cell Proteom*. 2022;21(2):100188–205.
 25. Yosudjai J, Inpad C, Chomwong S, Dana P, Sawanyawisuth K, Phimmsen S, Wongkham S, Jirawatnotai S, Kaewkong W. An aberrantly spliced isoform of anterior gradient-2, AGR2vH promotes migration and invasion of cholangiocarcinoma cell. *Biomed Pharmacother Biomed Pharmacother*. 2018;107:109–16.
 26. Fagerberg L, Hallstrom BM, Oksvold P, Kampf C, Djureinovic D, Odeberg J, Habuka M, Tahmasebpoor S, Danielsson A, Edlund K, et al. Analysis of the human tissue-specific expression by genome-wide integration of transcriptomics and antibody-based proteomics. *Mol Cell Proteom*. 2014;13(2):397–406.
 27. Neeb A, Hefele S, Bormann S, Parson W, Adams F, Wolf P, Miernik A, Schoenthaler M, Kroenig M, Wilhelm K, et al. Splice variant transcripts of the anterior gradient 2 gene as a marker of prostate cancer. *Oncotarget*. 2014;5(18):8681–9.
 28. Bergstrom JH, Berg KA, Rodriguez-Pineiro AM, Stecher B, Johansson ME, Hansson GC. AGR2, an endoplasmic reticulum protein, is secreted into the gastrointestinal mucus. *PLoS ONE*. 2014;9(8):e104186.
 29. Wodziak D, Dong A, Basin MF, Lowe AW. Anterior gradient 2 (AGR2) induced epidermal growth factor receptor (EGFR) signaling is essential for murine pancreatitis-associated tissue regeneration. *PLoS ONE*. 2016;11(10):e0164968.
 30. Zhao F, Edwards R, Dizon D, Afrasiabi K, Mastroianni JR, Geyfman M, Ouellette AJ, Andersen B, Lipkin SM. Disruption of paneth and goblet cell homeostasis and increased endoplasmic reticulum stress in *Aggr2*^{-/-} mice. *Dev Biol*. 2010;338(2):270–9.
 31. Li YP, Liu Y, Xiao LM, Chen LK, Tao EX, Zeng EM, Xu CH. Induction of cancer cell stemness in glioma through glycolysis and the long noncoding RNA HULC-activated FOXM1/AGR2/HIF-1 α axis. *Lab Invest*. 2022;102(7):691–701.
 32. Moidu NA, Rahman NSA, Syafruddin SE, Low TY, Mohtar MA. Secretion of pro-oncogenic AGR2 protein in cancer. *Heliyon*. 2020;6(9):e05000.
 33. Dahal Lamichane B, Jung SY, Yun J, Kang S, Kim DY, Lamichane S, Kim YJ, Park JH, Jang WB, Ji ST, et al. AGR2 is a target of canonical Wnt/ β -catenin signaling and is important for stemness maintenance in colorectal cancer stem cells. *Biochem Biophys Res Commun*. 2019;515(4):600–6.
 34. Tian SB, Tao KX, Hu J, Liu ZB, Ding XL, Chu YN, Cui JY, Shuai XM, Gao JB, Cai KL, et al. The prognostic value of AGR2 expression in solid tumours: a systematic review and meta-analysis. *Sci Rep*. 2017;7(1):15500–9.
 35. Valladares-Ayerbes M, Blanco-Calvo M, Reboredo M, Lorenzo-Patino MJ, Iglesias-Diaz P, Haz M, Diaz-Prado S, Medina V, Santamarina I, Pertega S, et al. Evaluation of the adenocarcinoma-associated gene AGR2 and the intestinal stem cell marker LGR5 as biomarkers in colorectal cancer. *Int J Mol Sci*. 2012;13(4):4367–87.
 36. Maarouf A, Boissard A, Henry C, Leman G, Coqueret O, Guette C, Lelievre E. Anterior gradient protein 2 is a marker of tumor aggressiveness in breast cancer and favors chemotherapy-induced senescence escape. *Int J Oncol*. 2022;60(1):5–19.
 37. Pan F, Li W, Yang W, Yang XY, Liu S, Li X, Zhao X, Ding H, Qin L, Pan Y. Anterior gradient 2 as a supervisory marker for tumor vessel normalization induced by anti-angiogenic treatment. *Oncol Lett*. 2018;16(3):3083–91.
 38. Tian S, Chu Y, Hu J, Ding X, Liu Z, Fu D, Yuan Y, Deng Y, Wang G, Wang L, et al. Tumour-associated neutrophils secrete AGR2 to promote colorectal cancer metastasis via its receptor CD98hc-xCT. *Gut*. 2022. <https://doi.org/10.1136/gutjnl-2021-325137>.
 39. Khan I, Baeesa S, Bangash M, Schulten HJ, Alghamdi F, Qashqari H, Madkhali N, Carracedo A, Saka M, Jamal A, et al. Pleomorphism and drug resistant cancer stem cells are characteristic of aggressive primary meningioma cell lines. *Cancer Cell Int*. 2017;17:72–86.
 40. Hussein D, Dallol A, Quintas R, Schulten HJ, Alomari M, Baeesa S, Bangash M, Alghamdi F, Khan I, ElAssouli MM, et al. Overlapping variants in the blood, tissues and cell lines for patients with intracranial meningiomas are predominant in stem cell-related genes. *Heliyon*. 2020;6(11):e05632.
 41. Xu C, Liu Y, Xiao L, Guo C, Deng S, Zheng S, Zeng E. The involvement of anterior gradient 2 in the stromal cell-derived factor 1-induced epithelial-mesenchymal transition of glioblastoma. *Tumour Biology*. 2016;37(5):6091–7.
 42. Latallo MJ, Livingston NM, Wu B. Translation imaging of single mRNAs in established cell lines and primary cultured neurons. *Methods*. 2019;162–163:12–22.
 43. Kalita O, Sporikova Z, Hajdud M, Megova Houdova M, Slavkovsky R, Hrabalek L, Halaj M, Klementova Y, Dolezel M, Drabek J, et al. The influence of gene aberrations on survival in resected IDH wildtype glioblastoma patients: a single-institution study. *Curr Oncol*. 2021;28(2):1280–93.
 44. Palande V, Siegal T, Detroja R, Gorohovski A, Glass R, Flueh C, Kanner AA, Laviv Y, Har-Nof S, Levy-Barda A, et al. Detection of gene mutations and gene-gene fusions in circulating cell-free DNA of glioblastoma patients: an avenue for clinically relevant diagnostic analysis. *Mol Oncol*. 2021;16(10):2098–114.
 45. Ambolet-Camoit A, Bui LC, Pierre S, Chevallier A, Marchand A, Coumoul X, Garlatti M, Andreau K, Barouki R, Aggerbeck M. 2,3,7,8-tetrachlorodibenzo-p-dioxin counteracts the p53 response to a genotoxicant by upregulating expression of the metastasis marker *agr2* in the hepatocarcinoma cell line HepG2. *Toxicol Sci*. 2010;115(2):501–12.
 46. Nguyen TTT, Zhang Y, Shang E, Shu C, Quinzii CM, Westhoff MA, Karpel-Massler G, Siegelin MD. Inhibition of HDAC1/2 Along with

- TRAP1 causes synthetic lethality in glioblastoma model systems. *Cells*. 2020;9(7):1661–78.
47. Wang N, Zhu P, Huang R, Sun L, Dong D, Gao Y. Suppressing TRAP1 sensitizes glioblastoma multiforme cells to temozolomide. *Exp Ther Med*. 2021;22(5):1246–54.
 48. Cho YA, Kim D, Lee B, Shim JH, Suh YL. Incidence, clinicopathologic, and genetic characteristics of mismatch repair gene-mutated glioblastomas. *J Neurooncol*. 2021;153(1):43–53.
 49. Skuladottir AT, Bjornsdottir G, Nawaz MS, Petersen H, Rognvaldsson S, Moore KHS, Olafsson PI, Magnusson SH, Bjornsdottir A, Sveinsson OA, et al. A genome-wide meta-analysis uncovers six sequence variants conferring risk of vertigo. *Commun Biol*. 2021;4(1):1148–56.
 50. Jiang L, Hao Y, Shao C, Wu Q, Prager BC, Gimple RC, Sulli G, Kim LJ, Zhang G, Qiu Z, et al. ADAR1-mediated RNA editing links ganglioside catabolism to glioblastoma stem cell maintenance. *J Clin Invest*. 2022;132(6):e143397.
 51. Yan Y, Takayasu T, Hines G, Dono A, Hsu SH, Zhu JJ, Riascos-Castaneda RF, Kamali A, Bhattacharjee MB, Blanco AI, et al. Landscape of genomic alterations in IDH wild-type glioblastoma identifies PI3K as a favorable prognostic factor. *JCO Precis Oncol*. 2020;4:575–84.
 52. Lombardo SD, Bramanti A, Ciurleo R, Basile MS, Pennisi M, Bella R, Mangano K, Bramanti P, Nicoletti F, Fagone P. Profiling of inhibitory immune checkpoints in glioblastoma: potential pathogenetic players. *Oncol Lett*. 2020;20(6):332–41.
 53. Cai X, Feng S, Zhang J, Qiu W, Qian M, Wang Y. USP18 deubiquitinates and stabilizes twist1 to promote epithelial-mesenchymal transition in glioblastoma cells. *Am J Cancer Res*. 2020;10(4):1156–69.
 54. Buruiana A, Florian SI, Florian AI, Timis TL, Mihu CM, Miclaus M, Osan S, Hrapasa I, Cataniciu RC, Farcas M, et al. The roles of miRNA in glioblastoma tumor cell communication: diplomatic and aggressive negotiations. *Int J Mol Sci*. 2020;21(6):1950–84.
 55. Rajesh Y, Biswas A, Kumar U, Das S, Banerjee I, Banik P, Bharti R, Nayak S, Ghosh SK, Mandal M. Targeting NFE2L2, a transcription factor upstream of MMP-2: a potential therapeutic strategy for temozolomide resistant glioblastoma. *Biochem Pharmacol*. 2019;164:1–16.
 56. Bailey MH, Tokheim C, Porta-Pardo E, Sengupta S, Bertrand D, Weerasinghe A, Colaprico A, Wendl MC, Kim J, Reardon B, et al. Comprehensive characterization of cancer driver genes and mutations. *Cell*. 2018;174(4):1034–5.
 57. Pratt D, Abdullaev Z, Papanicolaou-Sengos A, Ketchum C, Panneer Selvam P, Chung HJ, Lee I, Raffeld M, Gilbert MR, Armstrong TS, et al. High-grade glioma with pleomorphic and pseudopapillary features (HPAP): a proposed type of circumscribed glioma in adults harboring frequent TP53 mutations and recurrent monosomy 13. *Acta Neuropathol*. 2022;143(3):403–14.
 58. Rahane CS, Kutzner A, Heese K. A cancer tissue-specific FAM72 expression profile defines a novel glioblastoma multiform (GBM) gene-mutation signature. *J Neurooncol*. 2019;141(1):57–70.
 59. Eichberg DG, Slepak TI, Pascoini AL, Komotar RJ, Ivan ME. Genetic manipulation of adhesion GPCR CD97/ADGRE5 modulates invasion in patient-derived glioma stem cells. *J Neurooncol*. 2021;153(3):383–91.
 60. Estruch SB, Buzon V, Carbo LR, Schorova L, Luders J, Estebanez-Perpina E. The oncoprotein BCL11A binds to orphan nuclear receptor TLX and potentiates its transrepressive function. *PLoS ONE*. 2012;7(6):e37963.
 61. Liu J, Liu L, Xue Y, Meng F, Li S, Wang P, Liu Y. Anti-neoplastic activity of low-dose endothelial-monocyte activating polypeptide-II results from defective autophagy and G2/M arrest mediated by PI3K/Akt/FoxO1 axis in human glioblastoma stem cells. *Biochem Pharmacol*. 2014;89(4):477–89.
 62. Bueno-Martinez E, Lara-Almunia M, Rodriguez-Arias C, Otero-Rodriguez A, Garfias-Arjona S, Gonzalez-Sarmiento R. Polymorphisms in autophagy genes are genetic susceptibility factors in glioblastoma development. *BMC Cancer*. 2022;22(1):146–54.
 63. Zheng C, Wu H, Jin S, Li D, Tan S, Zhu X. Roles of Myc-associated zinc finger protein in malignant tumors. *Asia-Pacific J Clin Oncol*. 2022. <https://doi.org/10.1111/ajco.13748>.
 64. Schiapparelli P, Pirman NL, Mohler K, Miranda-Herrera PA, Zarco N, Kilic O, Miller C, Shah SR, Rogulina S, Hungerford W, et al. Phosphorylated WNK kinase networks in recoded bacteria recapitulate physiological function. *Cell Rep*. 2021;36(3):109416–45.
 65. Chen W, Zebaze LN, Dong J, Chezeau L, Inquimbert P, Hugel S, Niu S, Bihel F, Boutant E, Real E, et al. WNK1 kinase and its partners Akt, SGK1 and NBC-family Na(+)/HCO3(-) cotransporters are potential therapeutic targets for glioblastoma stem-like cells linked to Bisacodyl signaling. *Oncotarget*. 2018;9(43):27197–219.
 66. Park H, Jin UH, Karki K, Jayaraman A, Allred C, Michelhaugh SK, Mittal S, Chapkin RS, Safe S. Dopamine is an aryl hydrocarbon receptor agonist. *Biochem J*. 2020;477(19):3899–910.
 67. Sun Z, Shi S, Li H, Shu XH, Chen XY, Kong QY, Liu J. Evaluation of resveratrol sensitivities and metabolic patterns in human and rat glioblastoma cells. *Cancer Chemother Pharmacol*. 2013;72(5):965–73.
 68. Liu K, Tsung K, Attenello FJ. Characterizing cell stress and GRP78 in glioma to enhance tumor treatment. *Front Oncol*. 2020;10:608911–27.
 69. Delom F, Mohtar MA, Hupp T, Fessart D. The anterior gradient-2 interactome. *Am J Physiol Cell Physiol*. 2020;318(1):C40–7.
 70. Delom F, Nazaraliyev A, Fessart D. The role of protein disulphide isomerase AGR2 in the tumour niche. *Biol Cell*. 2018;110(12):271–82.
 71. Merugu SB, Zhou B, Mangukiya HB, Negi H, Ghulam R, Roy D, Qudisia S, Wang Z, Mashausi DS, Yunus FU, et al. Extracellular AGR2 activates neighboring fibroblasts through endocytosis and direct binding to beta-catenin that requires AGR2 dimerization and adhesion domains. *Biochem Biophys Res Commun*. 2021;573:86–92.
 72. Zhang Z, Li H, Deng Y, Schuck K, Raulefs S, Maeritz N, Yu Y, Hechler T, Pahl A, Fernandez-Saiz V, et al. AGR2-dependent nuclear import of RNA polymerase II constitutes a specific target of pancreatic ductal adenocarcinoma in the context of wild-type p53. *Gastroenterology*. 2021;161(5):1601–14.
 73. Grubelnik G, Bostjancic E, Groselj A, Zidar N. Expression of NANOG and its regulation in oral squamous cell carcinoma. *Biomed Res Int*. 2020;2020:8573793–804.
 74. Aran G, Sanjurjo L, Barcena C, Simon-Coma M, Tellez E, Vazquez-Vitali M, Garrido M, Guerra L, Diaz E, Ojanguren I, et al. CD5L is upregulated in hepatocellular carcinoma and promotes liver cancer cell proliferation and antiapoptotic responses by binding to HSPA5 (GRP78). *FASEB J*. 2018;32(7):3878–91.
 75. Lopez-Munoz E, Corres-Molina M, Garcia-Hernandez N. Correlation of the protein expression of GRP78 and BIK/NBK with prognostic markers in patients with breast cancer and neoadjuvant chemotherapy. *J Obstet Gynaecol*. 2020;40(3):419–26.
 76. Elinzano H, Toms S, Robison J, Mohler A, Carciari A, Cielo D, Donnelly J, Disano D, Vatketich J, Baekey J, et al. Nanoliposomal irinotecan and metronomic temozolomide for patients with recurrent glioblastoma: BrUOG329, a phase I brown university oncology research group trial. *Am J Clin Oncol*. 2021;44(2):49–52.
 77. Le Reste PJ, Pineau R, Voutetakis K, Samal J, Jegou G, Lhomond S, Gorman AM, Samali A, Patterson JB, Zeng Q, et al. Local intracerebral inhibition of IRE1 by MKC8866 sensitizes glioblastoma to irradiation/chemotherapy in vivo. *Cancer Lett*. 2020;494:73–83.
 78. Yang J, Zhang Q, Liu Y, Zhang X, Shan W, Ye S, Zhou X, Ge Y, Wang X, Ren L. Nanoparticle-based co-delivery of siRNA and paclitaxel for dual-targeting of glioblastoma. *Nanomedicine*. 2020;15(14):1391–409.
 79. Yuan P, Gu X, Ni X, Qi Y, Shao X, Xu X, Liu J, Qian X. Non-alkylator anti-glioblastoma agents induced cell cycle G2/M arrest and apoptosis: design, in silico physicochemical and SAR studies of 2-aminoquinoline-3-carboxamides. *Bioorg Med Chem Lett*. 2021;51:e128371.
 80. Kopa P, Maciejka A, Gulbas I, Pastwa E, Poplawski T. Inhibition of DNA-PK potentiates the synergistic effect of NK314 and etoposide combination on human glioblastoma cells. *Mol Biol Rep*. 2020;47(1):67–76.
 81. Graham-Gurysch EG, Murthy AB, Moore KM, Hingtgen SD, Bachelder EM, Ainslie KM. Synergistic drug combinations for a precision medicine approach to interstitial glioblastoma therapy. *J Controlled Release*. 2020;323:282–92.
 82. Schiariti MP, Restelli F, Ferrollo P, Benetti A, Berenzi A, Ferri A, Ceserani V, Cusani E, Cadei M, Finocchiaro G, et al. Fibronectin-adherent peripheral blood derived mononuclear cells as paclitaxel carriers for glioblastoma treatment: an in vitro study. *Cytotherapy*. 2017;19(6):721–34.
 83. Jach D, Cheng Y, Prica F, Dumartin L, Crnogorac-Jurcovic T. From development to cancer - an ever-increasing role of AGR2. *Am J Cancer Res*. 2021;11(11):5249–62.

84. Hong XY, Wang J, Li Z. AGR2 expression is regulated by HIF-1 and contributes to growth and angiogenesis of glioblastoma. *Cell Biochem Biophys*. 2013;67(3):1487–95.
85. Martisova A, Sommerova L, Kuricova K, Podhorec J, Vojtesek B, Kankova K, Hrstka R. AGR2 silencing contributes to metformin-dependent sensitization of colorectal cancer cells to chemotherapy. *Oncol Lett*. 2019;18(5):4964–73.
86. Kim SJ, Jun S, Cho HY, Lee DC, Yeom YI, Kim JH, Kang D. Knockdown of anterior gradient 2 expression extenuates tumor-associated phenotypes of SNU-478 ampulla of Vater cancer cells. *BMC Cancer*. 2014;14:804–13.
87. Zhang Y, Xia F, Zhang F, Cui Y, Wang Q, Liu H, Wu Y. miR-135b-5p enhances doxorubicin-sensitivity of breast cancer cells through targeting anterior gradient 2. *J Exp Clin Cancer Res*. 2019;38(1):26–38.
88. Jia M, Guo Y, Zhu D, Zhang N, Li L, Jiang J, Dong Y, Xu Q, Zhang X, Wang M, et al. Pro-metastatic activity of AGR2 interrupts angiogenesis target bevacizumab efficiency via direct interaction with VEGFA and activation of NF-kappaB pathway. *Biochim et Biophys Acta Mole Basis Dis*. 2018;1864(5):1622–33.
89. Hu Z, Gu Y, Han B, Zhang J, Li Z, Tian K, Young CY, Yuan H. Knockdown of AGR2 induces cellular senescence in prostate cancer cells. *Carcinogenesis*. 2012;33(6):1178–86.
90. Liu QG, Li YJ, Yao L. Knockdown of AGR2 induces cell apoptosis and reduces chemotherapy resistance of pancreatic cancer cells with the involvement of ERK/AKT axis. *Pancreatol*. 2018;18(6):678–88.
91. Murdocca M, Spitalieri P, De Masi C, Udroui I, Marinaccio J, Sanchez M, Talarico RV, Fiorillo C, D'Adamo M, Sbraccia P, et al. Functional analysis of POLD1 p.ser605del variant: the aging phenotype of MDPL syndrome is associated with an impaired DNA repair capacity. *Aging*. 2021;13(4):4926–45.
92. Lee E, Lee DH. Anterior gradient 2 is involved in the post-transcriptional regulation of beta-dystroglycan. *Anim Cells Syst*. 2021;25(1):19–27.
93. Gibieza P, Petrikaite V. The regulation of actin dynamics during cell division and malignancy. *Am J Cancer Res*. 2021;11(9):4050–69.
94. Alves MR, Melo NCE, Barros-Filho MC, do Amaral NS, Silva FIB, Baiocchi NG, Soares FA, de Brot AL, Rocha RM. Downregulation of AGR2, p21, and cyclin D and alterations in p53 function were associated with tumor progression and chemotherapy resistance in epithelial ovarian carcinoma. *Cancer Med*. 2018;7(7):3188–99.
95. Hrstka R, Bouchalova P, Michalova E, Matoulkova E, Muller P, Coates PJ, Vojtesek B. AGR2 oncoprotein inhibits p38 MAPK and p53 activation through a DUSP10-mediated regulatory pathway. *Mol Oncol*. 2016;10(5):652–62.
96. Echarri A. A multisensory network drives nuclear mechanoadaptation. *Biomolecules*. 2022;12(3):404–24.
97. Fahrenkrog B, Martinelli V, Nilles N, Fruhmans G, Chatel G, Juge S, Sauder U, Di Giacomo D, Mecucci C, Schwaller J. Expression of leukemia-associated Nup98 fusion proteins generates an aberrant nuclear envelope phenotype. *PLoS ONE*. 2016;11(3):e0152321.
98. Ma SR, Wang WM, Huang CF, Zhang WF, Sun ZJ. Anterior gradient protein 2 expression in high grade head and neck squamous cell carcinoma correlated with cancer stem cell and epithelial mesenchymal transition. *Oncotarget*. 2015;6(11):8807–21.

Publisher's Note

Springer Nature remains neutral with regard to jurisdictional claims in published maps and institutional affiliations.

Ready to submit your research? Choose BMC and benefit from:

- fast, convenient online submission
- thorough peer review by experienced researchers in your field
- rapid publication on acceptance
- support for research data, including large and complex data types
- gold Open Access which fosters wider collaboration and increased citations
- maximum visibility for your research: over 100M website views per year

At BMC, research is always in progress.

Learn more biomedcentral.com/submissions

